ACS APPLIED MATERIALS & INTERFACES

Research Article

www.acsami.org

Attempt to Improve the Performance of Pyrrole-Containing Dyes in Dye Sensitized Solar Cells by Adjusting Isolation Groups

Huiyang Li,[†] Yingqin Hou,[†] Yizhou Yang,[†] Runli Tang,[†] Junnian Chen,[†] Heng Wang,[‡] Hongwei Han,[‡] Tianyou Peng,[†] Qianqian Li,*[,†] and Zhen Li*[,†]

[†]Department of Chemistry, Hubei Key Lab on Organic and Polymeric Opto-Electronic Materials, Wuhan University, Wuhan 430072, China

[‡]Michael Grätzel Center for Mesoscopic Solar Cells, Wuhan National Laboratory for Optoelectronics, Huazhong University of Science and Technology, Wuhan, 430072, China

Supporting Information

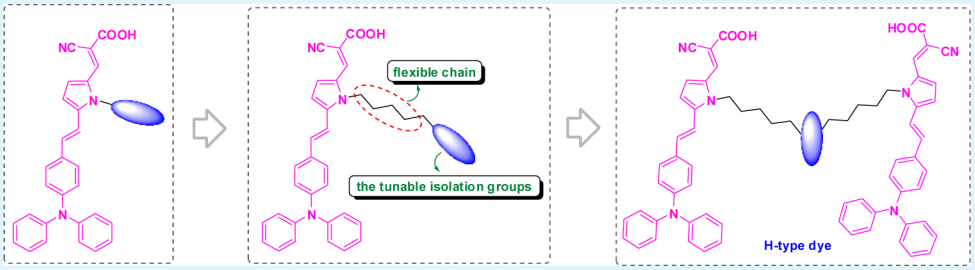

ABSTRACT: Four new pyrrole-based organic sensitizers with different isolation groups were conveniently synthesized and applied to dye sensitized solar cells (DSCs). The introduction of isolation group in the side chain could both suppress the formation of dye aggregates and electron recombination. Especially, when two pieces of D-π-A chromophore moieties shared one isolation group to construct the "H" type dye, the performance was further improved. Consequently, in the corresponding solar cell of **LI-57**, a short-circuit photocurrent density (J_{sc}) was tested to be 13.85 mA cm^{-2}, while 0.72 V for the open-circuit photovoltage (V_{oc}), 0.64 for the fill factor (FF), and 6.43% for the overall conversion efficiency (η), exceeding its analogue **LI-55** (5.94%) with the same isolation group. The results demonstrated that both the size (bulk and shape) and the linkage mode between the D-π-A chromophores and the isolation groups, could affect the performance of sensitizers in DSCs in a large degree, providing a new approach to optimize the chemical structure of dyes to achieve high conversion efficiencies.

KEYWORDS: *pyrrole, isolation group, "H" type dyes, organic sensitizer, dye-sensitized solar cell*

INTRODUCTION

Nowadays, many researchers around the world have taken on the challenge to solve the problem of the energy crisis, and the development of solar cell became one of the promising solutions.[1] Dye-sensitized solar cell (DSC) is a new generation photovoltaic (PV) device, and has attracted more and more attention since the report of Grätzel and O'Regan in 1991.[2] So far, by utilizing metal-complex sensitizers or perovskites, the power conversion efficiencies of solar cells have achieved to 15%.[3−6] In addition to the sensitizers containing precious metal, the metal-free organic dyes are another kind of promising alternative for DSCs, which possess some advantages including high molar absorption co-efficiencies, facile molecular tailoring, and cost-effectiveness.[7−11] However, until now, the conversion efficiencies of many pure organic dye sensitizers are still lower than those of metal complexes, the major factors should be the dye aggregates and the recombination of electrons in the semiconductor with the electrolyte or the oxidative dyes.[12] Actually, the formation of dye aggregates could, on one hand, result in the self-quenching of excited states, causing the followed inefficient electron injection, on another hand, accelerate the electron recombination. Both of them would lead to the unfavorable photovoltaic performance directly.[13−16] Moreover, the aggregation of dyes would influence the light absorption due to the presence of filtering effect.

As reported in the literatures,[17−20] the dye aggregates could be controlled in some degree through several strategies: the introduction of long alkyl chains to insulate dyes themselves on the TiO_2 surface;[21−25] the utilization of CDCA (chenodeoxycholic acid) to isolate dyes during the fabrication of DSCs.[26−28] However, generally, it would take a lot of time to explore an appropriate concentration of CDCA to achieve the optimized photovoltaic performance. In 2009, Ko et al. presented an alternative methodology to the immobilization of dyes on nanocrystalline TiO_2 electrodes,[29] in which dye molecules were encapsulated in cyclodextrin hosts. Such encapsulation could provide a means not only to prevent the

Received: August 30, 2013
Accepted: November 11, 2013
Published: November 11, 2013

formation of dye aggregates but also to retard the interfacial charge recombination dynamics. However, this supramolecular encapsulation strategy could only be applied to some limited dyes, in which cyclodextrins and the dyes should match each other to get an improved performance. Thus, it is still necessary to find other approaches to prevent the dye aggregation effectively.

With the aim to diminish the recombination of conduction-band electrons with the electrolyte and hinder the dye aggregation, we tried to improve the performance of DSCs through the molecular engineering.[30−32] In our previous work, we have prepared *N*-arylpyrrole-based organic dyes,[33] in which bulky non-coplanar aromatic rings were introduced to the pyrrole ring through the carbon−nitrogen single bonds on the nitrogen atom. This linkage mode could prevent the dye aggregation on the surface of TiO_2 effectively, however, nearly did not influence the D-π-A conjugated system. As a result, the solar cells based on *N*-arylpyrrole containing dyes exhibited good performance, with high V_{oc} value and long electron lifetime.[34] Actually, up to now, the usage of aromatic rings to optimize the performance of DSCs has been also reported by many other groups.[36−39] But, in most cases, the aromatic rings were linked to the donor part. Even in some cases that this rigid configuration was attached to the normal conjugated bridges, such as thiophene and phenyl group, usually, an adverse influence on the conjugation of the whole molecules was observed, resulting in the poor charge transfer throughout the whole molecule. Therefore, the modification of pyrrole-containing dyes is meaningful to prevent the dye aggregates, but without influencing the conjugation. Since the subtle difference in architectural design could be heavily related to their photovoltaic performance, it is still needed to investigate their detailed structure-property relationship. Deeply considering the previous work by us and other scientists, especially for a given D-π-A moieties, there is scare information on how to control the size of the isolation group, to obtain the optimized conversion efficiency. Thus, we wondered if there was an isolation group with suitable size for a given D-π-A conjugated system, to achieve an excellent performance. If there is, how about the linkage mode?

In this paper, we continued to optimize the structure of pyrrole based sensitizers by adjusting the size of the isolation group. We prepared some *N*-alkylpyrrole based dyes, **LI-54**−**LI-57** (Chart 1), in which, different isolation groups with different size were bonded to the end of the flexible side chain. The introduction of these isolation groups was expected to both suppress the aggregation of dyes on the surface of semiconductor and diminish the charge combination. Compared to *N*-arylpyrrole based organic dyes, in which the aromatic ring was bonded to the pyrrole ring on the nitrogen atom directly, the alkyl chain linked to the pyrrole ring would be more flexible for the dye orientation on the surface of the TiO_2 films. Fortunately, **LI-57** with the "H" structure, in which two pieces of D-π-A chromophore moieties shared one isolation group, showed the best performance: a V_{oc} of 0.72 V, a J_{sc} of 13.85 mA cm^{-2}, and a FF of 0.64, with a η value of 6.43%, about 1.26 times that of its analogue **LI-54**. Herein, we would like to present the syntheses of these *N*-alkylpyrrole based dyes, their structural characterization, the theoretical calculations, their electrochemical properties, and the photovoltaic performance of their corresponding solar cells in detail.

Chart 1. Structure of the Pyrrole-Containing Dyes LI-54−LI-57

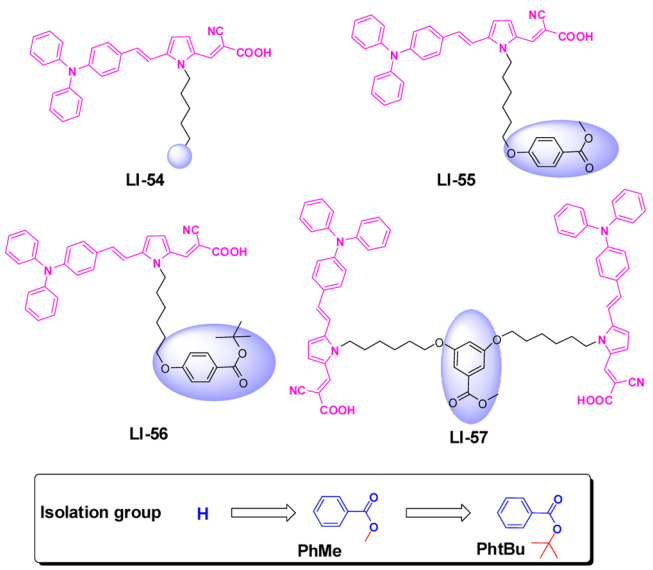

EXPERIMENTAL SECTION

Materials. Tetrahydrofuran (THF), *N*,*N*-dimethylformamide (DMF), and 1,2-dichloroethane were treated following the general procedure as previously, to remove the possible impurity and water.[31−34] Phosphorus oxychloride ($POCl_3$) was distilled before use. Compound **5** and diethyl 4-(diphenylamino)benzylphosphonate (**TPA-P**) was obtained according to the literatures.[40,41] All other reagents were purchased and used directly as received.

Instrumentation. A Varian Mercury 300 spectrometer was used to conduct ^1H and ^{13}C NMR spectroscopy by using tetramethylsilane (TMS; δ = 0 ppm) as internal standard. A ZAB 3F-HF mass spectrophotometer was used to measure MS (EI) spectra. A Finnigan LCQ advantage mass spectrometer was used to measure MS (ESI) spectra. A Shimadzu UV-2550 spectrometer was used to conduct UV-visible spectra. A CHI 660 voltammetric analyzer was used to conduct Electrochemical cyclic voltammetry, with Pt plate, Ag/Ag^+ electrode, and Pt disk, as counterelectrode, reference electrode, and working electrode, respectively, in anhydrous CH_2Cl_2 under an atmosphere of nitrogen, while the supporting electrolyte was tetrabutylammonium hexafluorophosphate ($TBAPF_6$) and a scanning rate was 100 mV/s. The potential calibration was conducted by using ferrocene/ferrocenium redox couple. A 73 CARLOERBA-1106 microelemental analyzer was used to conduct elemental analyses.

Synthesis. *General Procedure for the Preparation of **1b** and **1a**.* Under an atmosphere of nitrogen, KOH (3.4 equiv) was added to an anhydrous DMF (50 mL) solution of pyrrole-2-carbaldehyde (1 equiv) at 0 °C and stirred for half an hour. Then *n*-hexylbromide (1.2 equiv) or 1,6-dibromohexane (1.2 equiv) was added slowly. The mixture was reacted at 25 °C for 24 h, then poured into water (300 mL) and extracted with chloroform. The organic phase was combined, further washed with H_2O for three times, dried over sodium sulfate (Na_2SO_4), and purified through a silica chromatography column using ethyl acetate/petroleum (1:20) as an eluent.

1a. Light yellow liquid (4.24 g, 90.9%). ^1H NMR ($CDCl_3$) δ (ppm): 9.53 (s, 1H, ArH), 6.93 (s, br, 2H, ArH), 6.21 (s, 1H, ArH), 4.30 (t, J = 7.2 Hz, 2H, -*N*-CH_2−), 1.74 (s, br, −CH_2−, 2H), 1.28 (s, br, −CH_2−, 6H), 0.87 (t, J = 6.0 Hz, −CH_3, 3H).

1b. Light yellow liquid (1.90 g, 41.1%). ^1H NMR ($CDCl_3$) δ (ppm): 9.53 (s, ArH, 1H), 6.94 (s, br, ArH, 2H), 6.26 (d, J = 2.4 Hz, ArH, 1H), 4.31 (t, J = 7.2 Hz, -*N*-CH_2−, 2H), 3.39 (t, J = 6.9 Hz, 2H, −CH_2Br), 1.89−1.63 (m, −CH_2−, 4H), 1.48−1.26 (m, −CH_2−, 4H).

*General Procedure for the Preparation of **2b** and **2a**.* Under an atmosphere of dry nitrogen, potassium *tert*-butoxide (*t*-BuOK, 2.00 equiv) was added into an anhydrous tetrahydrofuran solution of

compound **4** (1.20 equiv), and the resultant mixture was reacted at 25 °C for 600 seconds. After the solution of **1a** or **1b** (1.00 equiv) in dry THF was added slowly, the mixture was stirred at 25 °C for 12 h, then poured into plenty of H_2O. $CHCl_3$ was used to extract the product for three times, and the organic layer was dried over sodium sulfate. After the removal of the organic solvent, the obtained solid was purified by column chromatography using petroleum/chloroform (10:1) as an eluent. The yielded solid was light sensitive, so once it was obtained, it was undergone another reaction in next step.

2a. Yellow oil (73.1%). ^{1}H NMR ($CDCl_3$) δ (ppm): 7.32 (d, J = 8.4 Hz, ArH, 2H), 7.28−7.22 (m, ArH and −CH═CH−, 4H), 7.10 (d, J = 7.2 Hz, ArH, 4H), 7.05−6.99 (m, 4H, ArH and −CH═CH−), 6.83 (s, 2H, ArH), 6.66 (s, 1H, ArH), 6.45 (s, 1H, ArH), 6.14 (s, ArH, 1H), 3.94 (t, J = 7.2 Hz, 2H, −N−CH_2−), 1.74 (s, br, 2H, −CH_2−), 1.31 (s, br, 6H, −CH_2−), 0.87 (s, br, −CH_3, 3H).

2b. Yellow oil (48.9%).^{1}H NMR ($CDCl_3$) δ (ppm): 7.32 (d, J = 8.7 Hz, ArH, 2H), 7.28-7.23 (m, ArH and −CH═CH−, 4H), 7.10 (d, J = 7.2 Hz, 4H, ArH), 7.05-6.99 (m, 4H, ArH and −CH═CH−), 6.83 (s, 2H, ArH), 6.65 (s, 1H, ArH), 6.45 (s, ArH, 1H), 6.15 (s, ArH, 1H), 3.96 (t, J = 6.6 Hz, −N−CH_2−, 2H), 3.37 (t, J = 6.6 Hz, −CH_2Br, 2H), 1.86−1.74 (m, 4H, −CH_2−), 1.49−1.33 (m, 4H, −CH_2−).

*General Procedure for the Preparation of **3b** and **3a***. Under an atmosphere of dry nitrogen, dry DMF (2.00 equiv) was added to phosphorus oxychloride (1.50 equiv) in an ice water bath, and the resultant solution was stirred to form a glassy solid. After **2a** or **2b** (1.00 equiv) in 1,2-dichloroethane was added, the mixture was reacted at 25 °C for 12 h, then poured into a sodium acetate solution in water. After stirred two hours, chloroform was used to extract the mixture for three times, and the combined organic layer was dried over sodium sulfate. After the removal of the solvent under vacuum, the yielded product was purified by flash chromatography using ethyl acetate/petroleum (1:10) as an eluent.

3a. Yellow oil (214 mg, 66.9%). ^{1}H NMR ($CDCl_3$) δ (ppm): 9.45 (s, −CHO, 1H), 7.36 (d, J = 8.1 Hz, ArH, 2H), 7.31−7.26 (m, 3H, ArH), 7.14−7.04 (m, ArH and −CH═CH−, 10H), 6.92 (d, J = 4.2 Hz, ArH, 1H), 6.84 (d, J = 15.6 Hz, −CH═CH−, 1H), 6.54 (d, J = 4.5 Hz, ArH, 1H), 4.45 (t, J = 7.5 Hz, −N−CH_2−, 2H), 1.73 (s, br, 2H, −CH_2−), 1.31 (s, br, −CH_2−, 6H), 0.87 (s, br, −CH_3, 3H).

3b. Yellow oil (600 mg, 48.9%). ^{1}H NMR ($CDCl_3$) δ (ppm): 9.44 (s, 1H, −CHO), 7.36 (d, J = 8.1 Hz, 2H, ArH), 7.31−7.26 (m, 3H, ArH), 7.14−7.04 (m, 10H, ArH and −CH═CH−), 6.92 (d, J = 4.2 Hz, 1H, ArH), 6.82 (d, J = 15.9 Hz, 1H, −CH═CH−), 6.54 (d, J = 3.9 Hz, 1H, ArH), 4.46 (t, J = 7.2 Hz, 2H, −N−CH_2−), 3.38 (t, J = 6.9 Hz, 2H, −CH_2Br), 1.87−1.73 (m, 4H, −CH_2−), 1.47−1.31 (m, 4H, −CH_2−).

*Synthesis of Sensitizer **LI-54***. A mixture of THF (5 mL), acetonitrile (10 mL), cyanoacetic acid (3.00 equiv), **3a** (1.00 equiv), and piperidine (10 μL) were added into a flask. The resultant mixture was reacted at 75 °C for 8 h. After it was cooled to room temperature, the resulted mixture was poured into 0.1 M HCl solution (100 mL). Chloroform was used to extract the crude product, and the combined organic layer was washed with H_2O for three times, and dried over sodium sulfate. After the removal of organic solvent, the obtained solid was purified by flash chromatography with $CHCl_3$/methanol (from 100:1 to 20:1) to yield a red solid. ^{1}H NMR ($CDCl_3$) δ (ppm): 8.04 (s, 1H, −CH═), 7.89 (d, J = 4.2 Hz, 1H, ArH), 7.37 (d, J = 8.7 Hz, 2H, ArH), 7.32−7.26 (m, 3H, ArH), 7.19−7.03 (m, 10H, ArH and −CH═CH−), 6.85−6.77 (m, 2H, ArH and −CH═CH−), 4.12 (s, br, 2H, −N−CH_2−), 1.73 (s, br, 2H, −CH_2−), 1.32 (s, br, 6H, −CH_2−), 0.88 (s, br, 3H, −CH_3). ^{13}C NMR (d_6-DMSO) δ (ppm): 166.3, 148.6, 147.9, 142.6, 138.9, 135.5, 133.7, 131.7, 130.8, 129.4, 128.3, 125.7, 124.8, 123.6, 120.1, 119.6, 115.1, 111.7, 43.5, 32.5, 31.9, 26.7, 23.2, 15.0. MS (EI): m/z calcd for $C_{34}H_{33}N_3O_2$: 515.64; found 471.23 [M − COOH]$^+$. Anal. Calcd for $C_{34}H_{33}N_3O_2$: C, 79.19; H, 6.45; N, 8.15. Found: C, 78.93; H, 6.21; N, 8.09.

*General Procedure for the Preparation of Compounds **6** and **7***. Methyl 4-hydroxybenzoate (1.50 equiv) or *tert*-butyl 4-hydroxybenzoate (1.50 equiv) with **3b** and KI (0.10 g), were added into a 100 mL round-bottom flask. To the flask was added acetone (20 mL) followed by K_2CO_3 (2.00 equiv). The mixture was refluxed overnight. After it was cooled to 25 °C, the product was isolated by filtration and further purified by column chromatography on silica gel using ethyl acetate/petroleum (1: 8) as an eluent.

6. Yellow solid (220 mg, 87.6%). ^{1}H NMR ($CDCl_3$) δ (ppm): 9.45 (s, 1H, −CHO), 7.95 (d, J = 8.4 Hz, 2H, ArH), 7.36 (d, J = 8.7 Hz, 2H, ArH), 7.30−7.26 (m, 3H, ArH), 7.13−7.03 (m, 10H, ArH and −CH═CH−), 6.92 (d, J = 4.2 Hz, 1H, ArH), 6.88−6.81(m, 3H, ArH and −CH═CH−), 6.54 (d, J = 3.9 Hz, 1H, ArH), 4.48 (t, J = 7.2 Hz, 2H, −N−CH_2−), 3.97 (t, J = 6.3 Hz, 2H, −OCH_2−), 3.88 (s, 3H, −OCH_3), 1.78 (s, br, 4H, −CH_2−), 1.46 (s, br, 4H, −CH_2−).

7. Yellow solid (595 mg, 78.8%). ^{1}H NMR ($CDCl_3$) δ (ppm): 9.44 (s, 1H, −CHO), 7.90 (d, J = 8.1 Hz, 2H, ArH), 7.36 (d, J = 8.7 Hz, 2H, ArH), 7.30−7.26 (m, 3H, ArH), 7.13−7.03 (m, 10H, ArH and −CH═CH−), 6.92 (d, J = 4.5 Hz, 1H, ArH), 6.85−6.82 (m, 3H, ArH and −CH═CH−), 6.54 (d, J = 3.6 Hz, 1H, ArH), 4.47 (t, J = 7.2 Hz, 2H, −N−CH_2−), 3.96 (t, J = 6.0 Hz, 2H, −OCH_2−), 1.80−1.76 (m, 4H, −CH_2−), 1.59 (s, 9H, −CH_3), 1.52−1.36 (m, 4H, −CH_2−).

*Synthesis of Compound **8***. Compound **8** was synthesized according to the similar procedure as **6** and **7** (262 mg, 66.7%).

8. Yellow solid. ^{1}H NMR ($CDCl_3$) δ (ppm): 9.44 (s, 2H, −CHO), 7.35 (d, J = 8.7 Hz, 4H, ArH), 7.29-7.26 (m, 6H, ArH), 7.12−7.02 (m, 22H, ArH and −CH═CH−), 6.91(d, J = 3.9 Hz, 2H, ArH), 6.83 (d, J = 16.2 Hz, 2H, −CH═CH−), 6.58−6.55 (m, 3H, ArH), 4.47 (s, br, 4H, −N−CH_2−), 3.92 (s, br, 4H, −OCH_2−), 3.87 (s, 3H, −OCH_3), 1.76 (s, br, 8H, −CH_2−), 1.44 (s, br, 8H, −CH_2−).

*Procedure for the Synthesis of Dye **LI-55**, **LI-56**, and **LI-57** through Knoevenagel Condensations*. **LI-55**, **LI-56**, and **LI-57** were obtained as dark red solid following the similar procedure to **LI-54**.

LI-55. Dark red solid (170 mg, 85.9%). ^{1}H NMR ($CDCl_3$) δ (ppm): 8.03 (s, 1H, −CH═), 7.95 (d, J = 8.1 Hz, 2H, ArH), 7.90 (d, J = 4.5 Hz, 1H, ArH), 7.37 (d, J = 8.1 Hz, 2H, ArH), 7.31−7.26 (m, 3H, ArH), 7.20−7.03 (m, 10H, ArH and −CH═CH−), 6.88−6.78 (m, 4H, ArH and −CH═CH−), 4.14 (s, br, 2H, −N−CH_2−), 3.98 (t, J = 5.7 Hz, 2H, −OCH_2−), 3.86 (s, 3H, −OCH_3), 1.79−1.77 (m, 4H, −CH_2−), 1.53 (s, br, 2H, −CH_2−), 1.43-1.41 (m, 2H, −CH_2−). ^{13}C NMR (DMSO-d_6) δ (ppm): 166.6, 165.8, 163.2, 148.1, 147.4, 142.3, 138.5, 133.3, 131.9, 131.1, 130.3, 128.9, 127.7, 125.1, 124.3, 122.9, 122.3, 119.8, 119.0, 115.0, 114.4, 111.3, 91.0, 68.4, 52.4, 43.4, 31.9, 29.0, 26.3, 25.7. MS (EI): m/z calcd for $C_{42}H_{39}N_3O_5$: 665.78; found 621.32 [M − COOH]$^+$. Anal. Calcd for $C_{42}H_{39}N_3O_5$: C, 75.77; H, 5.90; N, 6.31. Found: C, 75.52; H, 6.13; N, 5.95.

LI-56. Dark red solid (183 mg, 73.2%). ^{1}H NMR ($CDCl_3$) δ (ppm): 8.04 (s, 1H, −CH═), 7.91−7.89 (m, 3H, ArH), 7.37 (d, J = 8.4 Hz, 2H, ArH), 7.31−7.26 (m, 3H, ArH), 7.20−7.02 (m, 10H, ArH and −CH═CH−), 6.88−6.78 (m, 4H, ArH and −CH═CH−), 4.14 (s, br, 2H, −N−CH_2−), 3.96 (s, br, 2H, −OCH_2−), 1.77 (s, br, 4H, −CH_2−), 1.56 (s, 9H, −CH_3), 1.53−1.41(m, 4H, −CH_2−). ^{13}C NMR ($CDCl_3$) δ (ppm): 170.4, 165.8, 162.5, 148.6, 147.2, 138.4, 131.6, 131.5, 129.8, 129.6, 128.1, 127.9, 127.8, 125.3, 125.1, 124.8, 124.2, 123.8, 122.7, 113.9, 112.8, 80.6, 68.0, 43.2, 31.7, 29.1, 28.4, 26.6, 25.8. MS (EI): m/z calcd for $C_{45}H_{45}N_3O_5$ 707.86; found 663.39 [M − COOH]$^+$. Anal. Calcd for $C_{45}H_{45}N_3O_5$: C, 76.35; H, 6.41; N, 5.94. Found: C, 76.45; H, 6.25; N, 5.65.

LI-57. Dark red solid (89 mg, 39.5%). ^{1}H NMR (DMSO-d_6) δ (ppm): 8.01 (s, 2H, −CH═), 7.60−7.55 (m, 6H, ArH), 7.32−7.22 (m, 10H, ArH and −CH═CH−), 7.20 (d, J = 15.3 Hz, 2H, −CH═CH−), 7.08−6.96 (m, 14H, ArH), 6.89 (d, J = 8.7 Hz, 6H, ArH), 6.65 (s, 1H, ArH), 4.31 (s, br, 4H, −N−CH_2−), 3.88 (s, br, 4H, −OCH_2−), 3.78 (s, br, 3H, −OCH_3), 1.60 (s, br, 8H, −CH_2−), 1.40 (s, br, 4H, −CH_2−), 1.31 (s, br, 4H, −CH_2−). ^{13}C NMR ($CDCl_3$) δ (ppm): 170.6, 167.3, 160.2, 148.8, 147.3, 142.9, 138.4, 134.5, 132.0, 129.7, 128.2, 125.3, 124.0, 122.7, 122.1, 118.0, 112.6, 111.8, 108.0, 106.4, 88.9, 68.0, 52.6, 43.4, 31.9, 29.2, 26.7, 25.9. MS (ESI): m/z calcd for $C_{76}H_{70}N_6O_8$ 1195.4; found 1194.6 [M − H]$^+$. Anal. Calcd for $C_{76}H_{70}N_6O_8$: C, 76.36; H, 5.90; N, 7.03. Found: C, 76.39; H, 5.73; N, 6.95.

Device Fabrication and Photovoltaic Properties Measurements. The experimental conditions were similar to those reported previously.[34]

RESULTS AND DISCUSSION

Synthesis. In this work, the D-π-A moiety was similar to our previous study with triphenylamine acting as the donor, while pyrrole was selected as the bridge, and the acceptor and anchoring group was cyanoacetic acid. With the aim to optimize the performance of this structure, different isolation groups, which possessed different size, were introduced to the pyrrole rings through the alkyl chain. This linkage mode can cut off the conjugation effect between the D-π-A moiety and the isolation group completely, and the combination of the flexible chain and rigid structure can both prevent the $\pi-\pi$ stacking and reduce the charge recombination between the redox couple and the injected electrons in the TiO_2 film.

The synthetic approaches of the sensitizers were presented in Scheme 1. The corresponding units of aldehyde **1a** and **1b** were

Scheme 1

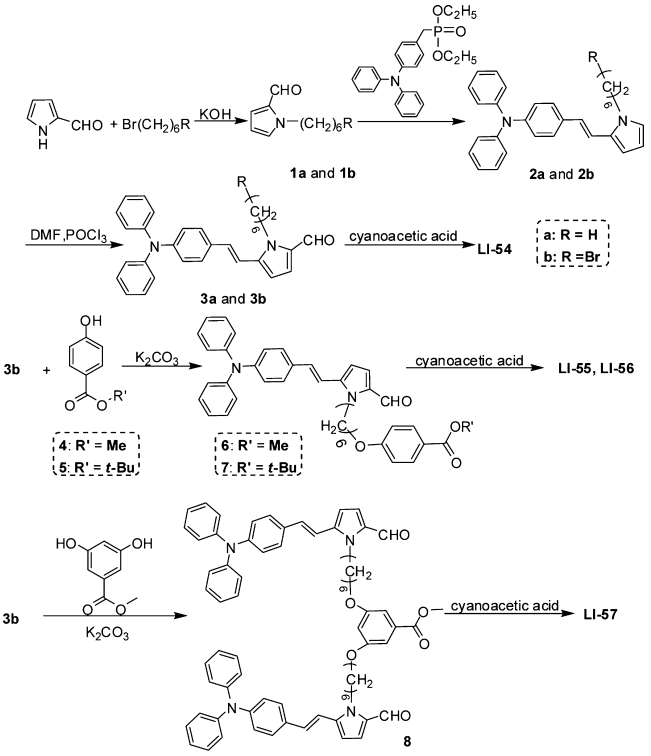

synthesized through a nucleophilic substitution reaction. Then, under a Wittig reaction between diethyl-4-(diphenylamino)-benzylphosphonate and **1a** or **1b**, compound **2a** and **2b** were obtained. Compound **2a** and **2b** are not so stable, thus, once they were obtained, both of them underwent the normal Vilsmeier reaction to yield **3a** and **3b**. Through a simple nucleophilic substitution reaction, various isolation groups were introduced into the intermediate aldehydes **6**, **7**, and **8** conveniently. Finally, in the presence of piperidine, the dyes were prepared from aldehydes **3a**, **6**, **7**, and **8** with cyanoacetic acid, through a Knoevenagel condensation reaction. The sensitizers and other compounds exhibited good solubility in common organic solvents (i.e., acetone, DMSO, CH_2Cl_2, DMF, $CHCl_3$, and THF). The structures of the compounds were confirmed by ^1H NMR, ^{13}C NMR, MS, and elemental analysis.

Optical Properties. Figure 1 demonstrated the absorption spectra of the dyes in diluted solution of CH_2Cl_2, and the absorption data were summarized in Table 1. In the UV−vis

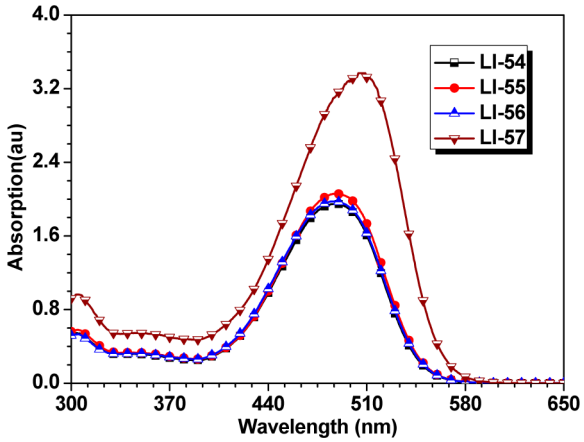

Figure 1. UV−vis spectra of sensitizers in dichloromethane. Concentration: 3.0×10^{-5} mol L^{-1}.

spectra, all of the dyes exhibited an intense absorption band at 400−600 nm, which should be attributed to an ICT process (intramolecular charge transfer) between the triphenylamine donor part and the acceptor of cyanoacetic acid. The absorbance of **LI-54**, **LI-55**, and **LI-56** was similar, while that of **LI-57** was nearly twice as high as that of the former ones, owning to the double light-harvesting units. There were no big differences in the maximum absorption peaks of the dyes **LI-54**, **LI-55**, and **LI-56**, indicating that the incorporation of isolation group at the end of side chain had little influence on the D-π-A conjugated systems. The absorption peak of **LI-57** showed a little red-shift, because of the intramolecular electron coupling of the double D-π-A moieties.

When absorbed on a transparent thin TiO_2 film, all dyes exhibited broader absorption spectra (Supporting Information Figure S1) than those in solution, as a result of the interaction between the carboxylate group and TiO_2. For the π^* orbital of the conjugated framework, this interaction could result in its increased delocalization, thus, the energy of the π^* level was decreased by this delocalization, resulting in the red-shifted absorption spectra.[15,22] The tail of their absorption spectra extended up to 620 nm, which was highly desirable to harvest more solar energy and translate into greater photocurrent.

The amounts of the adsorbed dye on the TiO_2 films were estimated by desorbing the dye with basic solution, and the surface concentrations of the four dyes were determined to be 1.97×10^{-7}, 1.74×10^{-7}, 1.75×10^{-7}, and 1.61×10^{-7} mol cm^{-2}, respectively (Table 1). Although **LI-57** had a large molecular size, which contained a couple of D-π-A moieties, its dye amount on the TiO_2 surface was just a little less than those of single D-π-A ones, indicating that the dye layer of **LI-57** on the TiO_2 surface was much more compact than others.

The anchoring properties of the dyes on the TiO_2 surface were investigate by the IR spectra (Supporting Information Figure S5), which were carried using the dye powder and dye-loaded TiO_2 films. As dye powders, the typical peak of the carboxylic acid group was located in the region of 1662−1671 cm^{-1}. Once adsorbed onto the TiO_2 surface, this carbonyl peak disappeared, however, the asymmetric (~1600 cm^{-1}) and symmetric stretching (~1370 cm^{-1}) bands for carboxylate units appeared, indicating that the four dyes were chemically adsorbed onto the TiO_2 surface via single- and double-anchoring modes, respectively. Considering the function of carbonyl unit in the chemical adsorption,[35] the ester units of

Table 1. Electrochemical Properties and Absorbance of Sensitizers

sensitizer	λ_{max}[a] (nm)	λ_{max}[b] (nm)	dye loading[c] ($\times 10^{-7}$ mol cm^{-2})	$E_{0\text{-}0}$[d] (eV)	E_{ox}[e] (V) NHE	E_{red}[f] (V) NHE	E_{LUMO}[g] (eV)	E_{HOMO}[g] (eV)
LI-54	487	506	1.94	2.21	0.90	−1.31	−2.99	−5.00
LI-55	488	506	1.74	2.21	0.92	−1.29	−3.01	−5.02
LI-56	486	501	1.75	2.21	0.99	−1.22	−3.08	−5.09
LI-57	504	501	1.61	2.16	0.95	−1.21	−3.09	−5.05

[a]Absorption spectra of sensitizers measured in dichloromethane (3×10^{-5} mol L^{-1}). [b]Absorption spectra of sensitizers adsorbed on the TiO_2 surface. [c]The dye loading was determined from a dye-loaded 15 μm thick TiO_2 film. [d]The bandgap, E_{0-0}, was calculated from the observed optical edge. [e]E_{ox} were measured in CH_2Cl_2. The oxidation potential (E_{ox}) (referenced Ag/AgCl) was converted to the NHE reference scale: $E_{ox} = E_{ox}^{on} + 0.2$ V. [f]E_{red} was calculated from $E_{ox} - E_{0-0}$. [g]The HOMO was taken from the first redox potential in CV plot, the LUMO was calculated with the expression of LUMO = HOMO − E_{0-0}.

the isolation groups have also drawn some attention. The ester peaks in the region of 1705−1716 cm^{-1} maintained, when the dyes were absorbed on the TiO_2 surface, partly suggesting that the isolation group did not anchor on the TiO_2 surface.

Electrochemical Properties. In DSCs, the electron injection is very important from the excited dyes to the conduction band of TiO_2, also, the dye regeneration by the iodide is essential. And the energy levels of the organic dyes are important criterion for these possibilities. Generally, the oxidation potential (E_{ox}) measured by cyclic voltammetry (Supporting Information Figure S3) was corresponded to the highest occupied molecular orbital (HOMO), and the reduction potential (E_{red}), was corresponded to the lowest unoccupied molecular orbital (LUMO) (Table 1). In the voltammograms, we could observe two oxidation waves. The first quasi-reversible oxidation waves at lower oxidation potentials, were attributed to the triphenylamine, while the higher oxidation potentials with quasi-reversible behavior, were from the spacer, pyrrole rings. The HOMO levels of the dyes, taken from the first oxidation potential, were lower than −4.80 eV, which was about the redox potential of the I^-/I_3^- redox couple, making enough driving force for the reduction of oxidized dyes. The LUMO levels of the sensitizers were much higher than −4.00 eV, which was the conduction band edge energy level (E_{cb}) of the TiO_2 electrode, energetically permitting the electron injection from the excited sensitizer into the conduction band of TiO_2. It should be noted that all the sensitizers had the similar HOMO and LUMO levels, infering that the introduced isolation group did not affect the D-π-A conjugated system, in good accordance with our expectation.

Theoretical Calculations. To know more about the correlation between the structure and properties, we further conducted quantum chemistry computation (Figure 2): optimizing the geometries of the dyes using DFT calculations with Gaussian 09 program,[42] analyzing the structures of the dyes using a B3LYP/6-31G* hybrid functional for full geometrical optimization. In the ground state, the D-π-A system of the dyes had a nearly coplanar conformation to realize a maximal extent of π-delocalization, and the dihedral angles between pyrrole unit and its neighboring units (Supporting Information Figure S5) were less than 25°, meaning that the isolation group bonded to the end of the side chain did not impact the conjugation along the chromophore moieties. From frontier orbital electron density distributions, it could be seen that, for all dyes, the HOMO orbital was mainly located on the TPA donor and the conjugated bridge, whereas for the LUMO, it was localized in the cyanoacetic acid and the conjugated bridge but concentrated on the acceptor. The results indicated that the ICT induced by light moved the electron density from the TPA donor to cyanoacetic acid acceptor, thus allowing an efficient photoinduced electron transfer from the sensitizer to the TiO_2 electrode.

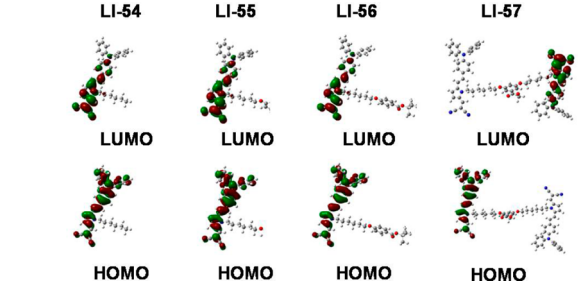

Figure 2. Frontier orbitals of the dyes optimized at the B3LYP/6-31G*level.

Photovoltaic Performance of DSCs. The photovoltaic characteristics of the sensitizer-based DSCs were measured with a sandwich DSC cell comprising I_2 (0.05 M), butylmethylimidazolium iodide (BMII, 0.6 M), lithium iodide (0.1 M), and 4-*tert*-butylpyridine (4-TBP, 0.5 M) in the mixed solvents of 3-methoxypropionitrile and acetonitrile (7:3, v/v) as the redox electrolyte. The procedure for the device preparation and characterization were presented in the Experimental Section. Figure 3 plotted the incident photon-to-electron conversion efficiencies (IPCE), which is a function of incident wavelength for the corresponding DSCs of the resulting organic dyes on TiO_2 films. As easily seen, the dyes were active in the wavelength region (350-650 nm). It should be noted that the

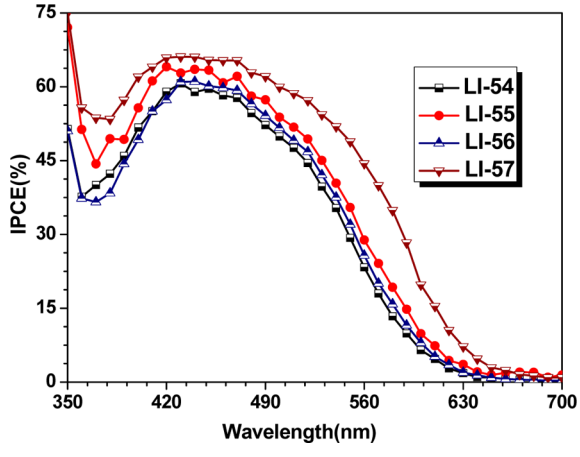

Figure 3. Spectra of monochromatic IPCE for DSCs of these sensitizers.

IPCE values increased in the order of **LI-54** < **LI-56** ≈**LI-55** < **LI-57**. As the dyes had the same D-π-A conjugated system, the different IPCE values should be certainly ascribed to the different isolation groups of the dyes. **LI-54** was a rod shaped dye with only alkyl chain in the side, reasonably, the strong intermolecular $\pi-\pi$ interaction would exist once absorbed onto the TiO_2 surface, which usually led to the inefficient electron injection caused by the self-quenching of excited states. **LI-55** and **LI-56**, with PhMe and PhtBu as the rigid unit linked to the end of the alkyl chain, respectively, had the higher values than **LI-54**, indicating that a single side chain failed to exhibit the efficient anti-aggregation, whereas the introduction of suitable isolation group was more effective in decreasing the $\pi-\pi$ interaction between dyes and thus increasing the IPCE values. In principle, the larger size of the isolation group, the better isolation effect for the anti-aggregation. However, the isolation group would not influence the light absorption, thus, the larger isolation group, the relatively lower concentration of the effective D-π-A moieties, which would result in the lower IPCE values. So, a balance should be present between these two points, and a suitable isolation group should be there to optimize the performance of the dye with the fixed structure of D-π-A. Actually, this opinion could be confirmed by the results of dyes **LI-54**–**LI-56**. As mentioned above, the IPCE values of **LI-55** and **LI-56** were higher than that of **LI-54** because of the introduced isolation group. In comparison with that of **LI-55**, the value of **LI-56** was a little lower, although it contained the larger isolation group of PhtBu. This indicated that the size of PhMe might be suitable enough for this kind of dyes, **LI-54**–**LI-56**.

Previously, we have designed a series of "H"-type dyes, in which two pieces of D-π-A chromophore moieties were linked together through various aromatic rings.[34] These dyes demonstrated good performance and the configuration of "H"-type could prevent the dye aggregation on the TiO_2 surface. Here, the IPCE value of **LI-55** disclosed that PhMe might be the suitable isolation group for **LI-54**–**LI-56**. Then, how about the usage of PhMe as the isolation group between two pieces of D-π-A chromophore moieties, to construct a new "H"-type dye? Perhaps, combined with the suitable size of PhMe and the special "H" configuration, the resultant dye could exhibit even better performance. Really, the IPCE value of **LI-57** was higher than that of **LI-55**, partially realizing our idea.

Figure 4 showed the current-voltage characteristics of DSCs employing the isolating type dyes as sensitizers, which were tested under standard global AM 1.5 solar light conditions. The photovoltaic characteristic parameters of open-circuit voltage (V_{oc}), short-circuit current density (J_{sc}), fill factor (FF), and photovoltaic conversion efficiency (η) were listed in Table 2. The **LI-54** sensitized solar cell produced a J_{sc} of 11.30 mA cm^{-2}, a V_{oc} of 0.69 V, and a FF of 0.66, corresponding to a η of 5.12%. In the case of **LI-55**, the J_{sc} value (11.31 mA cm^{-2}) was higher than that of **LI-54** under the same conditions and the V_{oc} was further improved to 0.72 V, finally leading to a photovoltaic conversion efficiency of 5.94%. Since the two dye sensitizers had the same conjugated system, the contribution to J_{sc} and final photovoltaic conversion efficiency should be assigned to the isolation group (PhMe). Changing the isolation group from PhMe to PhtBu, **LI-56** showed a poorer performance than that of **LI-55**, demonstrating that the size of the isolation group have noticeable impact on their photovaltic properties. Actually, the introduced isolation

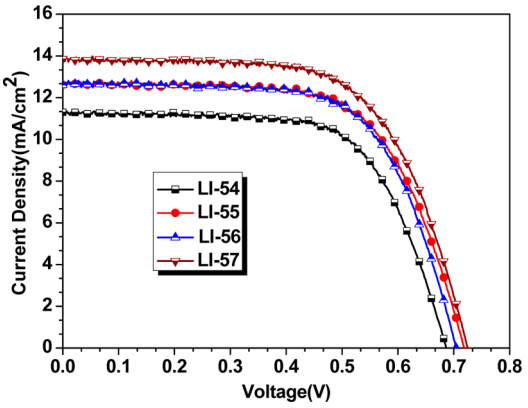

Figure 4. $J-V$ characteristics of DSCs measured at simulated 100 mW cm^{-2} AM1.5 conditions.

Table 2. Dye Sensitized Solar Cell Performance Data of Dyes

sensitizer	J_{sc} (mA cm^{-2})	V_{oc} (V)	FF	η (%)
LI-54	11.30	0.69	0.66	5.12
LI-55	12.61	0.72	0.65	5.94
LI-56	12.60	0.70	0.67	5.88
LI-57	13.85	0.72	0.64	6.43

group had two opposite effects: on one hand, the isolation group can separate the D-π-A conjugated system to aviod the possible aggregate and electron coupling, which was benificial to the arrangement of the dyes on the TiO_2 surface; on the other hand, the isolation group can not absorb the light, reducing the light-harvesting capability of the whole molecule. Thus, it was significant to adjust the bulky size of the isolation group to match the fixed D-π-A moieties, with the aim to achieve the optimal conversion efficiency. For this conjugation skeleton, the size of PhtBu unit may be a little too big, while that of PhMe was suitable. Keeping this group as the isolation group again, and attaching two same D-π-A moieties together, the resultant **LI-57** offered a J_{sc} of 13.85 mA cm^{-2}, a V_{oc} of 0.72 V, and a FF of 0.64, corresponding to a η of 6.43%, which was the highest value of these four dyes, with the same trend of IPCE values. Analyzing the results carefully, it could be seen that the high conversion efficiency of **LI-57** was mostly due to the increased J_{sc} value (Figure 5), indicating that the structure with two pieces of D-π-A moieties together in one molecule would increase the density of the light-harvesting unit

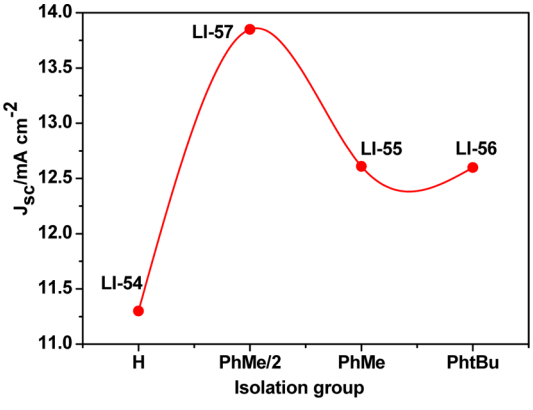

Figure 5. Comparison of the J_{sc} values of the sensitizers with different sizes of isolation groups.

effectively, additionally, the isolation group between them could prevent the possible $\pi-\pi$ stacking or electron recombination in a large degree. So, the excellent performance of **LI-57** sensitized solar cell was reasonable, confirming the advantages of "H" type dyes again.

Since CDCA could bind strongly to nanostructured TiO_2, making the reacting points for dye molecules on the semiconductor surface less and therefore hindering the aggregation of dyes. When severe aggregates formed on the surface of TiO_2, upon coadsorption of CDCA, they could act as isolation spacers among dye sensitizers and thus suppressed their possible $\pi-\pi$ interactions, which can retard the charge recombination between the injected electrons in TiO_2 film and the electrolyte. Thus, in severe aggregates cases, regardless that the amount of dyes on the TiO_2 surface was reduced through coadsorption with CDCA, the conversion efficiency usually increased.[43,44] To get more information of the relationship between the conversion efficiency and the structure of the dye sensitizers, we studied the influence of the coadsorption of CDCA on their photovoltaic properties. For the coadsorption, both 5 mM and 10 mM CDCA was added. The performances of the DSCs in the presence of CDCA with various concentrations were collected in Supporting Information Table S1, while the corresponding $J-V$ curves were shown in Supporting Information Figure S4. For **LI-54** based DSC, the J_{sc} value kept soaring with the increasing concentration of CDCA (from 11.30 to 12.23, 12.45 mA cm^{-2}), because of the presence of CDCA to suppress the aggregation of dye **LI-54**. As dye sensitizers in the monomer form could inject electrons to TiO_2 more efficiently than aggregate, low concentration of CDCA failed to work well for **LI-54** and it needed higher concentration of CDCA for the coadsorption to obtain high J_{sc} value. Or in other word, the relatively severe aggregation of dye **LI-54** existed on the TiO_2 surface, hinting that the alkyl chains as the side group could not separate the dyes effectively. Once the rigid group have been incorporated into the side group, for **LI-55** and **LI-56** based DSCs, when the concentration of CDCA was 5 mM, the J_{sc} values increased a little, further increase its concentration to 10 mM, they decreased, especially for **LI-56**, J_{sc} dropped from 13.69 to 12.72 mA cm^{-2}, exhibiting that the concentration of CDCA (10 mM) was too high for the two dyes, and in this case, CDCA decreased the dye loading on the TiO_2 surface, resulting in the reduction of photocurrent density. The tiny increase of J_{sc} values, when the CDCA concentration was decrease to 5 mM, indicated that only slight aggregates or electron recombination formed in **LI-55** and **LI-56** sensitized solar cells, suggesting that the incorporation of aromatic rings at the end of the alkyl chain as an isolation group in **LI-55** and **LI-56** could suppress the dye aggregates on the TiO_2 surface more effectively than a single alkyl chain in pristine dye, **LI-54**. Interestingly, in the case of **LI-57**, CDCA did not improve the performance of the device, and the J_{sc} decreased with the increasing concentration of CDCA. This H-type dye, **LI-57**, featuring double D-π-A conjugation system with aromatic rings at the end of the alkyl chain, could suppress aggregation itself on the surface of TiO_2 in a large degree, thus there was no need for the addition of CDCA to improve the performance of the devices. The presence of CDCA was bad for the arrangement of the dye **LI-57**, and decreased the light-harvesting units, finally led to the poorer performance.

Electrochemical Impedance Spectroscopy. Under a forward bias of −0.70 V with a frequency range of 0.1 Hz to 100 kHz, we measured the electrochemical impedance spectroscopy (EIS) in the dark, to elucidate the correlation of V_{oc} with the dyes. The Nyquist plots and Bode phase plots of the DSCs based on the sensitizers were shown in Figure 6. In

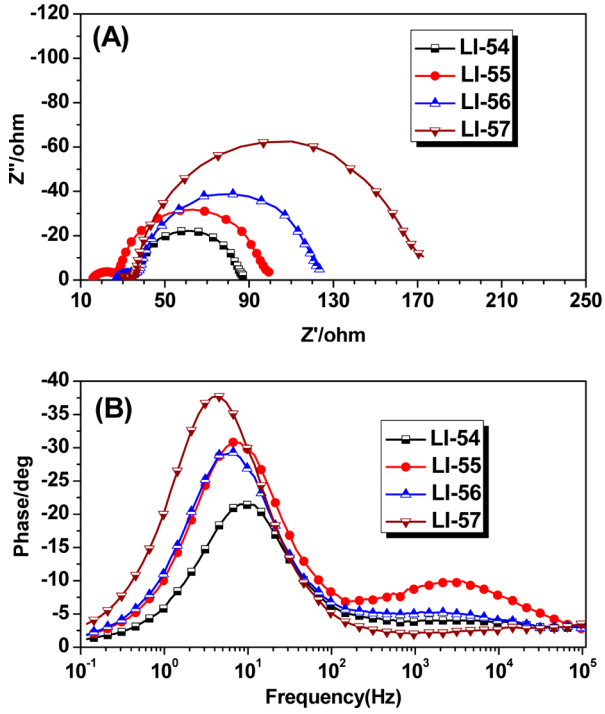

Figure 6. Electrochemical impedance spectroscopy for DSCs of the sensitizers. (A) Nyquist plots in the dark and (B) Bode phase plots in the dark.

the Nyquist plot, the large semicircle at the intermediated frequency was assigned to the charge transfer impedance at the TiO_2/dye/electrolyte interface. The charge recombination resistance at the TiO_2 surface, R_{rec}, could be estimated from the radius of the middle semicircle in the Nyquist plot, and the larger R_{rec} meant a slower charge recombination rate. As shown in Figure 6A, **LI-55** and **LI-56** with rigid isolation groups presented larger radius of the middle semicircle than **LI-54**. And **LI-57**, in which two pieces of chromophore moieties shared one isolation group, showed the largest R_{rec}. The increased R_{rec} values implied the retardation of charge recombination between the injected electron into the TiO_2 and oxidized species (I_3^-) in the electrolyte, further showing the superiority of the special configuration of **LI-57**. The characteristic frequency in the Bode plot was concerned on the charge recombination rate, also, its reciprocal was related to the electron lifetime. Correspondingly, the characteristic frequency peaks in the Bode phase plots increased in the order of **LI-54** > **LI-55** ≈ **LI-56** > **LI-57**, suggesting that the aromatic rings at the end of the alkyl chain contributed to the enhanced electron lifetime, due to the formation of a dense blocking dye layer, resulting in a higher V_{oc}. These results were consistent with the tendency of V_{oc} in the DSCs based on the synthesized dyes.

CONCLUSION

A series of pyrrole-based pure organic sensitizers with different isolation groups were designed and synthesized. Excitingly, it was found that both the size and the linkage mode of the isolation groups had a large influence on their performance, providing a new approach to achieve higher conversion

efficiency by choosing a suitable isolation group to control the alignment of the dyes on the surface of TiO_2. Among the four dyes, **LI-57** with "H" configuration and one isolation group (PhMe), showed the best performance, with a J_{sc} of 13.85 mA cm^{-2}, a V_{oc} of 0.72 V, and a FF of 0.64, corresponding to a η of 6.43% without the addition of CDCA.

■ ASSOCIATED CONTENT

Ⓢ Supporting Information

Figures of UV−vis spectra on TiO_2 film, IR spectra, cyclic voltammograms, and $J-V$ characteristics of DSCs with different concentrations of CDCA. This information is available free of charge via the Internet at http://pubs.acs.org.

■ AUTHOR INFORMATION

Corresponding Authors

*Phone: 86-27-62254108. Fax: 86-27-68756757. E-mail: qianqian-alinda@163.com,
*Phone: 86-27-62254108. Fax: 86-27-68756757. E-mail: lizhen@whu.edu.cn, lichemlab@163.com.

Notes

The authors declare no competing financial interest.

■ ACKNOWLEDGMENTS

We are grateful to the National Science Foundation of China (21002075 and 21372003), and the National Fundamental Key Research Program (2011CB932702) for financial support.

■ REFERENCES

(1) Grätzel, M. *Nature* **2001**, *414*, 338−344.
(2) O'Regan, B.; Grätzel, M. *Nature* **1991**, *353*, 737−740.
(3) Burschka, J.; Pellet, N.; Moon, S.-J.; Humphry-Baker, R.; Gao, P.; Nazeeruddin, M. K.; Grätzel, M. *Nature* **2013**, *499*, 316−319.
(4) Kim, H. S.; Mora-Sero, I.; Gonzalez-Pedro, V.; Fabregat-Santiago, F.; Juarez-Perez, E. J.; Park, N. G.; Bisquert, J. *Nat. Chem.* **2013**, DOI: 10.1038/ncomms3242.
(5) Yella, A.; Lee, H.-W.; Tsao, H. N.; Yi, C.; Chandiran, A. K.; Nazeeruddin, Md. K.; Diau, E. W.-G.; Yeh, C.-Y.; Zakeeruddin, S. M.; Grätzel, M. *Science* **2013**, *334*, 629−633.
(6) Liu, M.; Johnston, M. B.; Snaith, H. J. *Nature* **2013**, *501*, 395−398.
(7) Zhu, W.; Wu, Y.; Wang, S.; Li, W.; Li, X.; Chen, J.; Wang, Z.; Tian, H. *Adv. Funct. Mater.* **2011**, *21*, 756−763.
(8) Liang, M.; Chen, J. *Chem. Soc. Rev.* **2013**, *42*, 3453−3488.
(9) Wu, Y.; Zhu, W. *Chem. Soc. Rev.* **2013**, *42*, 2039−2058.
(10) Cai, N.; Wang, Y.; Xu, M.; Fan, Y.; Li, R.; Zhang, M.; Wang, P. *Adv. Funct. Mater.* **2013**, *23*, 1846−1854.
(11) Zhang, G.; Bala, H.; Cheng, Y.; Shi, D.; Lv, X.; Yu, Q.; Wang, P. *Chem. Commun.* **2009**, 2198−2200.
(12) Zhang, S.; Yang, X.; Numata, Y.; Han, L. *Energy Environ. Sci.* **2013**, *6*, 1443−1464.
(13) Numata, Y.; Islam, A.; Chen, H.; Han, L. *Energy Environ. Sci.* **2012**, *5*, 8548−8552.
(14) Ren, X.; Jiang, S.; Cha, M.; Zhou, G.; Wang, Z.-S. *Chem. Mater.* **2012**, *24*, 3493−3499.
(15) Tang, J.; Hua, J.; Wu, W.; Li, J.; Jin, Z.; Long, Y.; Tian, H. *Energy Environ. Sci.* **2010**, *3*, 1736−1745.
(16) Qin, C.; Islam, A.; Han, L. *J. Mater. Chem.* **2012**, *22*, 19236−19243.
(17) Wu, Z.; An, Z.; Chen, X.; Chen, P. *Org. Lett.* **2013**, *15*, 1456−1459.
(18) Ting, H.-C.; Tsai, C.-H.; Chen, J.-H.; Lin, L.-Y.; Chou, S.-H.; Wong, K.-T.; Huang, T.-W.; Wu, C.-C. *Org. Lett.* **2012**, *14*, 6338−6341.
(19) Chen, H.; Huang, H.; Huang, X.; Clifford, J. N.; Forneli, A.; Palomares, E.; Zheng, X.; Zheng, L.; Wang, X.; Shen, P.; Zhao, B.; Tan, S. *J. Phys. Chem. C* **2010**, *114*, 3280−3286.
(20) Qin, H.; Wenger, S.; Xu, M.; Gao, F.; Jing, X.; Wang, P.; Zakeeruddin, S. M.; Grätzel, M. *J. Am. Chem. Soc.* **2008**, *130*, 9202−9203.
(21) Zeng, W.; Cao, Y.; Bai, Y.; Wang, Y.; Shi, Y.; Zhang, M.; Wang, F.; Pan, C.; Wang, P. *Chem. Mater.* **2010**, *22*, 1915−1925.
(22) He, J.; Guo, F.; Li, X.; Wu, W.; Yang, J.; Hua, J. *Chem.—Eur. J.* **2012**, *18*, 7903−7915.
(23) Pei, K.; Wu, Y.; Wu, W.; Zhang, Q.; Chen, B.; Tian, H.; Zhu, W. *Chem.—Eur. J.* **2012**, *18*, 8190−8200.
(24) Li, S.-R.; Lee, C.-P.; Kuo, H.-T.; Ho, K.-C.; Sun, S.-S. *Chem.—Eur. J.* **2012**, *18*, 12085−12095.
(25) Wang, C.; Fang, Y.; Cao, Z.; Huang, H.; Zhao, B.; Li, H.; Liu, Y.; Tan, S. *Dyes Pigm* **2013**, *97*, 405−411.
(26) Shi, J.; Chen, J.; Chai, Z.; Wang, H.; Tang, R.; Fan, K.; Wu, M.; Han, H.; Qin, J.; Peng, T.; Li, Q.; Li, Z. *J. Mater. Chem.* **2012**, *22*, 18830−18838.
(27) Ying, W.; Guo, F.; Li, J.; Zhang, Q.; Wu, W.; Tian, H.; Hua, J. *ACS Appl. Mater. Interfaces* **2012**, *4*, 4215−4224.
(28) Yang, J.; Guo, F.; Hua, J.; Li, X.; Wu, W.; Qu, Y.; Tian, H. *J. Mater. Chem.* **2012**, *22*, 24356−24365.
(29) Choi, H.; Kang, S. O.; Ko, J.; Gao, G.; Kang, H. S.; Kang, M.-S.; Nazeeruddin, M. K.; Grätzel, M. *Angew. Chem., Int. Ed.* **2009**, *48*, 5938−5941.
(30) Shi, J.; Chai, Z.; Zhong, C.; Wu, W.; Hua, J.; Dong, Y.; Qin, J.; Li, Q.; Li, Z. *Dyes Pigm.* **2012**, *95*, 244−251.
(31) Li, Q.; Lu, L.; Zhong, C.; Shi, J.; Huang, Q.; Jin, X.; Peng, T.; Qin, J.; Li, Z. *J. Phys. Chem. B* **2009**, *113*, 14588−14595.
(32) Shi, J.; Huang, J.; Tang, R.; Chai, Z.; Hua, J.; Qin, J.; Li, Q.; Li, Z. *Eur. J. Org. Chem.* **2012**, 5248−5255.
(33) Li, Q.; Lu, L.; Zhong, C.; Huang, J.; Huang, Q.; Shi, J.; Jin, X.; Peng, T.; Qin, J.; Li, Z. *Chem.—Eur. J.* **2009**, *15*, 9664−9668.
(34) Li, Q.; Shi, J.; Li, H.; Li, S.; Zhong, C.; Guo, F.; Peng, M.; Hua, J.; Qin, J.; Li, Z. *J. Mater. Chem.* **2012**, *22*, 6689−6696.
(35) Mao, J.; He, N.; Ning, Z.; Zhang, Q.; Guo, F.; Chen, L.; Wu, W.; Hua, J.; Tian, H. *Angew. Chem. Int. Ed.* **2012**, *51*, 9873−9876.
(36) Wang, C.-L.; Lan, C.-M.; Hong, S.-H.; Wang, Y.-F.; Pan, T.-Y.; Chang, C.-W.; Kuo, H.-H.; Kuo, M.-Y.; Diau, E. W.-G.; Lin, C.-Y. *Energy Environ. Sci.* **2012**, *5*, 6933−6940.
(37) Li, L.-L.; Diau, E. W.-G. *Chem. Soc. Rev.* **2013**, *42*, 291−304.
(38) Duan, T.; Fan, K.; Zhong, C.; Peng, T.; Qin, J.; Chen, X. *RSC Adv.* **2012**, *2*, 7081−7086.
(39) Wu, H.-P.; Ou, Z.-W.; Pan, T.-Y.; Lan, C.-M.; Huang, W.-K.; Lee, H.-W.; Reddy, N. M.; Chen, C.-T.; Chao, W.-S.; Yeh, C.-Y.; Diau, E. W.-G. *Energy Environ. Sci.* **2012**, *5*, 9843−9848.
(40) Iqbal, P.; Critchley, K.; Bowen, J.; Attwood, D.; Tunnicliffe, D.; Evans, S. D.; Preece, J. A. *J. Mater. Chem.* **2007**, *17*, 5097−5110.
(41) Zheng, S.; Barlow, S.; Parker, T. C.; Marder, S. R. *Tetrahedron Lett.* **2003**, *44*, 7989−7992.
(42) Frisch, M. J.; Trucks, G. W.; Schlegel, H. B.; Scuseria, G. E.; Robb, M. A.; Cheeseman, J. R.; Scalmani, G.; Barone, V.; Mennucci, B.; Petersson, G. A.; Nakatsuji, H.; Caricato, M.; Li, X.; Hratchian, H. P.; Izmaylov, A. F.; Bloino, J.; Zheng, G.; Sonnenberg, J. L.; Hada, M.; Ehara, M.; Toyota, K.; Fukuda, R.; Hasegawa, J.; Ishida, M.; Nakajima, T.; Honda, Y.; Kitao, O.; Nakai, H.; Vreven, T.; Montgomery, J. A., Jr.; Peralta, J. E.; Ogliaro, F.; Bearpark, M.; Heyd, J. J.; Brothers, E.; Kudin, K. N.; Staroverov, V. N.; Kobayashi, R.; Normand, J.; Raghavachari, K.; Rendell, A.; Burant, J. C.; Iyengar, S. S.; Tomasi, J.; Cossi, M.; Rega, N.; Millam, J. M.; Klene, M.; Knox, J. E.; Cross, J. B.; Bakken, V.; Adamo, C.; Jaramillo, J.; Gomperts, R.; Stratmann, R. E.; Yazyev, O.; Austin, A. J.; Cammi, R.; Pomelli, C.; Ochterski, J. W.; Martin, R. L.; Morokuma, K.; Zakrzewski, V. G.; Voth, G. A.; Salvador, P.; Dannenberg, J. J.; Dapprich, S.; Daniels, A. D.; Farkas, O.; Foresman, J. B.; Ortiz, J. V.; Cioslowski, J.; Fox, D. J. *Gaussian 09*; Gaussian, Inc.: Wallingford, CT, 2009.
(43) Wang, Z.-S.; Cui, Y.; Dan-oh, Y.; Kasada, C.; Shinpo, A.; Hara, K. *J. Phys. Chem. C* **2007**, *111*, 7224−7230.

(44) Ren, X.; Feng, Q.; Zhou, G.; Huang, C.-H.; Wang, Z.-S. *J. Phys. Chem. C* **2010**, *114*, 7190−7195.